Biogeosciences Discuss., 5, 5093–5132, 2008
www.biogeosciences-discuss.net/5/5093/2008/

Biogeosciences Discussions

Biogeosciences Discussions is the access reviewed discussion forum of *Biogeosciences*

Distributions of surface water CO_2 and air-sea flux of CO_2 in coastal regions of the Canadian Beaufort Sea in late summer

A. Murata[1], K. Shimada[2], S. Nishino[1], and M. Itoh[1]

[1]Institute of Observational Research for Global Change (IORGC), Japan Agency for Marine-Earth Science and Technology (JAMSTEC), 2-15, Natsushima, Yokosuka, Kanagawa 237-0061, Japan
[2]Department of Ocean Sciences, Tokyo University of Marine Science and Technology, 4-5-7, Konan, Minato-ku, Tokyo 108-8477, Japan

Received: 7 October 2008 – Accepted: 15 October 2008 – Published: 18 December 2008

Correspondence to: A. Murata (murataa@jamstec.go.jp)

Published by Copernicus Publications on behalf of the European Geosciences Union.

Abstract

To quantify the air-sea flux of CO_2 in a high-latitude coastal region, we conducted shipboard observations of atmospheric and surface water partial pressures of CO_2 (pCO_2) and total dissolved inorganic carbon (TCO_2) in the Canadian Beaufort Sea (150° W–127° W; 69° N–73° N) in late summer 2000 and 2002. Surface water pCO_2 was lower than atmospheric pCO_2 (2000, 361.0 μatm; 2002, 364.7 μatm), and ranged from 250 to 344 µatm. Accordingly, ΔpCO_2, which is the driving force of the air-sea exchange of CO_2 and is calculated from differences in pCO_2 between the sea surface and the overlying air, was generally negative (potential sink for atmospheric CO_2), although positive ΔpCO_2 values (source) were also found locally. Distributions of surface water pCO_2, as well as those of ΔpCO_2 and CO_2 flux, were controlled mainly by water mixing related to river discharge. The air-sea fluxes of CO_2 were −15.0 and −16.8 mmol m^{-2} d^{-1} on average in 2000 and 2002, respectively, implying that the area acted as a moderate sink for atmospheric CO_2. The air-to-sea net CO_2 flux in an extended area of the western Arctic Ocean (411 000 km^2) during the ice-free season (=100 days) was calculated as 10.2±7.7 mmol m^{-2} d^{-1}, equivalent to a regional CO_2 sink of 5.0±3.8 Tg C. The estimated buffer factor was 1.5, indicating that the area is a high-capacity CO_2 sink. These CO_2 flux estimates will need to be revised because they probably include a bias due to the vertical gradients of physical and chemical properties characteristic in the region, which have not yet been adequately considered.

1 Introduction

Atmospheric CO_2 is now increasing at the rate of 1.9 ppmv yr^{-1} (Solomon et al., 2007) by emissions of CO_2 resulting from human activities such as consumption of fossil fuels, deforestation, and cement production. CO_2 that originates from human activities is called anthropogenic CO_2. Accurate estimation of the uptake of anthropogenic CO_2 by the ocean is an urgent task for the scientific community, which has undertaken the task

BGD

5, 5093–5132, 2008

of forecasting global warming and relevant climate changes in the near future. For this reason, anthropogenic CO_2 uptake by the ocean has been evaluated by using several approaches: model calculations (Le Quéré et al., 2000; Obata and Kitamura, 2003; Wetzel et al., 2005), global integration of air-sea fluxes of CO_2 calculated from field observations (Takahashi et al., 2002), and water column inventory of anthropogenic CO_2 (Sabine et al., 2004). Currently, it is estimated that the ocean and the terrestrial biosphere absorb about 50% of anthropogenic CO_2, with each absorbing a similar amount (Solomon et al., 2007).

The Arctic Ocean has not been taken into account sufficiently in the global estimation of the CO_2 budget in the ocean, because, in addition to sparse data coverage, it has been plausibly inferred that the air-sea exchange of CO_2 in the Arctic Ocean is negligible owing to the presence of sea-ice during a long period of each year. However, we should nevertheless evaluate CO_2 uptake in the Arctic Ocean because (1) CO_2 is expected to have high solubility because of the low water temperature, and (2) seas adjacent to the Arctic Ocean lie above continental shelves, where biological production is high. These factors operate to reduce the surface water pCO_2 to a level much lower than the atmospheric CO_2 level. Accordingly, it is likely that the Arctic Ocean acts a substantial sink for atmospheric CO_2 in spite of its brief ice-free period. Furthermore, the area covered by sea ice is reducing rapidly (Rothrock et al., 1999; Stroeve et al., 2005), which implies that the area for air-sea exchange of CO_2 is increasing. In fact, it has been reported that uptake of CO_2 by the Arctic Ocean has tripled over the last three decades as a result of sea-ice retreat (Bates et al., 2006).

The Arctic Ocean, especially its surface layer, is subject to physical and biogeochemical processes such as cooling, stratification, water mixing, primary production, and respiration. These processes jointly affect carbon dynamics in the Arctic Ocean, although the relative importance of the different processes differs from region to region. Thus, it is important to elucidate the dominant process controlling CO_2 dynamics in the Arctic Ocean to estimate more accurately its uptake of CO_2.

The present study aimed to examine air-sea exchange of CO_2 in coastal regions of

BGD
5, 5093–5132, 2008

the Canadian Beaufort Sea. As part of this examination, we clarified the influence of river discharge, mostly from the Mackenzie River, on the CO_2 dynamics in the region. Spatial variations in oceanic CO_2 in western Arctic Ocean seas, west of 150° W, have been previously reported (Murata and Takizawa, 2003). The present study focused on the area east of 150° W using data obtained during cruises in 2000 (Murata and Takizawa, 2003) and 2002. We also point out that it is likely that the vertical oceanic structural characteristics in the region cause a bias in the estimated air-sea CO_2 flux.

2 Data and methods

2.1 Data

Data used in the present study were obtained by shipboard observations in the western Arctic Ocean during the MR00-K06 (13–22 September 2000) and MR02-K05 (15–30 September 2002) cruises (Fig. 1) of the R/V *Mirai* of the Japan Agency for Marine-Earth Science and Technology (JAMSTEC). For details of the cruises, please refer to the cruise reports (http://www.jamstec.go.jp/cruisedata/mirai/e/index.html).

Atmospheric and surface water mole fractions of CO_2 (xCO_2 in ppmv) were measured continuously by a nondispersive infrared gas analyzer system installed in the research vessel. The CO_2 standard gases used to calibrate the system on board the *Mirai* were calibrated against gases from the Scripps Institution of Oceanography (SIO). The precision of the atmospheric and surface water xCO_2 measurements was estimated to be 0.2 and 1.7 ppmv, respectively, for 2000, and 0.2 and 1.0 ppmv, respectively, for 2002. The xCO_2 values were converted to partial pressures of CO_2 (pCO_2 in µatm) under saturated water vapor pressure at sea surface temperature (SST) by using an air pressure of 1.0 atm and the SST. The saturated water vapor pressure was computed according to Weiss and Price (1980). The xCO_2 and pCO_2 data used in the present study will be made available to the public through the Surface Ocean CO_2 Atlas (SOCAT) project of the International Ocean Carbon Coordination Project

(http://www.ioccp.org).

Surface water total dissolved inorganic carbon (TCO_2) was also measured continuously by the system with a coulometer installed on the R/V *Mirai*. The precision was estimated to be 1.6 and 2.0 µmol kg^{-1} for the 2000 and 2002 cruises, respectively. The TCO_2 data were recalibrated by using a certified reference material (CRM) provided by A. G. Dickson of SIO.

For details of the analytical methods, please refer to Murata and Takizawa (2003).

Both onboard systems for pCO_2 and TCO_2 independently recorded SST and sea surface salinity (SSS) at the sampling time of each property. In addition to the underway observations, chemical properties such as TCO_2 and total alkalinity (TAlk) in the water column were measured at conductivity-temperature-depth (CTD) stations during both cruises (Fig. 1).

2.2 Calculation of TAlk

Surface water TAlk was calculated from surface water pCO_2 and TCO_2, which were measured continuously on board the *Mirai*. Since sampling times of the measured properties were different, data adjustment for the calculation was necessary; first, data for pCO_2, TCO_2, SST and SSS measured within ±30 min of hours were averaged. Then, TAlk (µmol kg^{-1}) on hours was calculated from the averaged pCO_2, TCO_2, SST, and SSS values by using Eq. (1):

$$\mathrm{TAlk} = [HCO_3^-] + 2[CO_3^{2-}] + [B(OH)_4^-] + [OH^-] - [H^+] - [HSO_4^-] - [HF], \quad (1)$$

where the square brackets [ ] indicate the concentration (µmol kg^{-1} in seawater) of each respective species. Dissociation constants necessary for the calculation were taken from Weiss (1974) for the solubility coefficient of CO_2 in seawater, Goyet and Poisson (1989) for the first and second dissociation constants, Dickson (1990a) for boric acid, Millero (1995) for water, Dickson (1990b) for bisulfate ion and Dickson and Riley (1979) for hydrogen fluoride.

The actual calculations were done using an MS Excel® version of the software program of Lewis and Wallace (1998) created by Dr. D. Pierrot. The calculated TAlk adequately represents the temporal and spatial variations during the cruises because the averaged pCO_2 could be used to reconstruct variations of nonaveraged surface water pCO_2 without any loss of major variation patterns.

The data set for pCO_2, TCO_2, and TAlk was used examine the spatial variability of surface water pCO_2 from the viewpoint of the oceanic carbonate system (Sect. 4.2).

2.3 Calculation of the air-sea flux of CO_2

The net air-sea flux of CO_2, F (mmol m^{-2} d^{-1}), was computed with Eq. (2):

$$F = k \cdot s(\Delta pCO_2), \quad (2)$$

where k (cm h^{-1}) indicates the transfer velocity, s (mol kg^{-1} atm^{-1}) is the solubility of CO_2 (Weiss, 1974), and ΔpCO_2 is calculated by subtracting atmospheric pCO_2 values from surface water pCO_2 values. For atmospheric pCO_2, we used averages of measured values in the study area: 361.0 and 364.7 µatm for 2000 and 2002, respectively (Table 1).

How to reliably parameterize k is still debated (Ho et al., 2006), and several formulas have been used in actual calculations of CO_2 fluxes. However, the most frequently used formulas may be those of Liss and Merlivat (1986) and Wanninkhof (1992) (hereafter abbreviated as W92). In the present study, we used the formula of W92 for the following analysis.

According to W92, there is a quadratic relationship between wind speed w (m s^{-1}) and transfer velocity k:

$$k = 0.31(w_{10})^2(Sc/660)^{-0.5}, \quad (3)$$

where w_{10} is wind speed at 10 m elevation and Sc is the Schmidt number, which we calculated using the equation given by Wanninkhof (1992). The wind speeds used for

the calculation of the CO_2 fluxes were measured on board the *Mirai* during the cruises. For comparison with the CO_2 fluxes reported in previous studies, we also show the results calculated using the parameterization of Liss and Mertlivat (1986), Wanninkhof and McGillis (1999), Nightingale et al. (2000), and Ho et al. (2006).

3 Results

3.1 Distributions of surface water pCO_2 and related properties

The basic statistics for atmospheric CO_2 are summarized in Table 1. Mean atmospheric xCO_2 was 363.2 ± 1.8 in 2000 and 367.0 ± 1.4 ppmv in 2002, values which are close to the monthly mean (September) obtained at Point Barrow (Alaska, USA). Surface water pCO_2 (Table 2) shows variations about 10-fold those of atmospheric pCO_2. Mean surface water pCO_2 was calculated as 292.1± 22.1 and 306.5±27.6 µatm for 2000 and 2002, respectively. Although the means, standard deviations, and minima differed little between the years, the surface water pCO_2 maxima differed markedly between 2000 (395.4 µatm) and 2002 (490.0 µatm).

Distributions of surface water pCO_2, surface water TCO_2, calculated surface water TAlk, SST, and SSS in 2000 are shown in Fig. 2a–e, respectively, as a function of sequential day. We use sequential day to display variations in the properties to eliminate overlap, which would occur if we plotted the properties by longitude and latitude.

Surface water pCO_2 was mostly lower than atmospheric pCO_2 (361.0 µatm) except around day 260 (Fig. 2a). The highest surface seawater pCO_2 was measured near the mouth of the Mackenzie River. Surface water TCO_2 and SST (Fig. 2b and d) were positively correlated with surface water pCO_2 from the initial day to around day 263, whereas SSS variations (Fig. 2e) were negatively correlated during the same period. TAlk (Fig. 2c) also varied positively with surface water pCO_2, although its variations were less pronounced, probably at least in part because the smaller number of the calculated TAlk values led to a lower time and space resolution. Around day 263,

BGD
5, 5093–5132, 2008

pCO_2 decreased abruptly by approximately 50 µatm, whereas on about the same day, the other properties increased.

Distributions of surface water pCO_2, surface water TCO_2, calculated surface water TAlk, SST, and SSS in 2002 are shown in Fig. 3a–e, respectively, as a function of sequential day. As in 2000, surface water pCO_2 (Fig. 3a) was usually lower than atmospheric pCO_2 (364.7 µatm), although supersaturation of surface water pCO_2 was observed locally. In 2002, shipboard observations were made near the mouth of the Mackenzie River on two different legs of the cruise: legs 3 and 5 (Fig. 1b'). Around day 263 on leg 3, surface water pCO_2 decreased by about 50 µatm concurrently with decreases in TCO_2, TAlk, and SSS (Fig. 3b, c, and e) and with an increase in SST (Fig. 3d). On leg 5, however, a similar distinct relationship among the properties cannot be discerned. Instead, the properties all showed relatively higher variability during leg 5 than during the other legs. On leg 4, TCO_2, TAlk, and SSS distributions exhibit V-shaped valleys, but SST exhibits a peak (an inverted V). In spite of these changes, surface water pCO_2 was approximately constant at 320 µatm during leg 4.

In summary, surface water pCO_2 was mostly undersaturated with respect to atmospheric pCO_2, as 97% of the observations (n=2561) in the two years were between 250 and 344 µatm.

3.2 Air-sea exchanges of CO_2

ΔpCO_2, the driving force of air-sea exchange of CO_2 calculated as the difference of pCO_2 between the sea surface and the overlying air (the latter is subtracted from the former), was mostly negative in both years except in areas close to the mouth of the Mackenzie River, where it became positive, reaching +125 µatm at maximum (2002). The averaged ΔpCO_2 was −68.8±22.2 and −58.2±27.6 µatm in 2000 and 2002, respectively (Table 3). The ΔpCO_2 distribution displayed the same patterns as the relationship between atmospheric and surface water pCO_2 each year (Figs. 2a and 3a).

CO_2 flux distributions in 2000 calculated using the W92 formulation are shown as a function of sequential day in Fig. 4a. The CO_2 fluxes were generally negative except

around day 260, when observations were made near the mouth of the Mackenzie River (Fig. 1a'). The averaged CO_2 flux in 2000 was $-15.0\,mmol\,m^{-2}\,d^{-1}$ (Table 3).

CO_2 flux distributions in 2002 are displayed in Fig. 4b. During the first three legs in 2002, the CO_2 fluxes were consistently negative but close to zero, whereas in the during legs 4, 5, and 6, large negative fluxes with high variability were observed. The averaged CO_2 flux in 2002 was $-16.8\,mmol\,m^{-2}\,d^{-1}$ (Table 3), nearly the same as that in 2000. Nevertheless, the temporal and spatial variability of the CO_2 flux was larger in 2002 than in 2000, as is clear from the standard deviations (Table 3). In 2002, large positive CO_2 fluxes were also observed during leg 5, when observations were made near the mouth of the Mackenzie River (Fig. 1b'), whereas in 2000, such a large positive CO_2 fluxes were not observed.

In summary, the area overall acted as a moderate sink for atmospheric CO_2, although sea-to-air CO_2 fluxes were observed locally.

4 Discussion

As reported in Sect. 3.1, the dynamic range of surface water pCO_2 was larger than that of atmospheric CO_2, implying that spatial variations of ΔpCO_2 were controlled chiefly by the variations in surface water pCO_2. Hence, it is important to elucidate the cause of the spatial variations in surface water pCO_2 to assess where future sinks or sources of atmospheric CO_2 might exist, when an ice-free period becomes longer as expected.

As a possible cause of the spatial variations in pCO_2, we first examine biological processes (production and remineralization), using observed and calculated chemical properties, and demonstrate that these effects cannot primarily account for the distribution of surface water pCO_2 (Sect. 4.1). Next, we investigate spatial variations in pCO_2 in relation to water mixing, especially river discharge, which is a dominant process in the study area (Sect. 4.2). Then, we discuss differences in calculated air-sea fluxes of CO_2 between 2000 and 2002, and between the areas east and west of 150° W. We also estimate the CO_2 fluxes in the area as a whole (Sect. 4.3). Lastly, we evaluate

BGD
5, 5093–5132, 2008

the capacity of the study area as a CO_2 sink on the basis of the so-called buffer factor (Sect. 4.4).

4.1 Biological processes

Because of the high biological productivity of coastal regions (Codispoti et al., 1986) and the patchiness of biological activity (Valiela, 1995), biogeochemical processes can cause high spatial variations in pCO_2. For example, from spring to summer, the drawdown of pCO_2 in the Chuckchi Sea, to the west of the Beaufort Sea, is known to be related to biological production (Bates et al., 2005).

A simple method of estimating biological production is to calculate net community production (NCP; $mg\,C\,m^{-2}\,d^{-1}$), which can be estimated from convenient chemical properties such as dissolved oxygen, nitrate, and TCO_2. In fact, NCP has been repeatedly used to quantify biological production (Codispoti et al., 1986; Murata et al., 2002; Bates et al., 2005). If it is calculated from TCO_2, NCP is obtained by dividing the drawdown of TCO_2 normalized to a salinity of 35 ($\Delta nTCO_2$) by the duration (days) of production. NCP becomes positive when net autotrophic processes exceed net heterotrophic processes (Hansell and Carlson, 1998). In the study area, $\Delta nTCO_2$ can be estimated from the difference of $nTCO_2$ between the surface and the temperature minimum layer (TML) in the upper ocean, because the temperature minimum water is regarded as a remnant of winter water (Coachman et al., 1975; Midorikawa et al., 2002). Using this method, NCP from the end of the previous winter to the observation time is roughly estimated by assuming a constant decrease of $nTCO_2$ in the surface layer from winter to spring. However, during this study (Fig. 5), $nTCO_2$ in the surface layer was consistently higher than that in the TML; that is, no drawdown of $nTCO_2$ relative to the TML value was observed in the layers above the TML in the study area. This result implies that the surface water pCO_2 in the study area is little controlled by biological production during CO_2-rich conditions in wintertime followed by drawdown of CO_2 in the subsequent season, as is often found elsewhere, such as in the northwestern North Pacific (Murata et al., 2002) and the Southern Ocean (Ishii et al., 1998).

BGD
5, 5093–5132, 2008

As we discuss in Sect. 4.2, higher concentrations of $nTCO_2$ were associated with river discharge. Thus, we discuss here the possibility that biological processes in the river discharge are a factor causing the observed spatial variations of surface water pCO_2.

To investigate biological activity affecting distributions of surface water pCO_2, we plotted the TCO_2 to TAlk ratio (TCO_2/TAlk) as a function of salinity (Fig. 6). The TCO_2/TAlk ratio is usually determined by in situ changes in TCO_2, that is, production and remineralization of organic matter. We found that the ratio generally decreased linearly with increasing salinity, although two trends (i.e., a break in the slope at a salinity of about 22) can be seen in 2000 (Fig. 6a), and considerable variation from the expected trend are seen in 2002 (Fig. 6b). The anomalously higher TCO_2/TAlk ratios found at lower salinity, that is, near the mouth of the Mackenzie River (Fig. 6b), may imply the presence of water (river discharge) with a larger degree of net heterotrophy. Biological activity in the river, for example, in the delta (Emmerton et al., 2008) could possibly cause net heterotrophy. However, the generally conservative changes in the TCO_2/TAlk ratio (Fig. 6) indicate that net heterotrophic processes do not continue after the low-salinity river water mixes with the coastal region waters.

The nitrate-depleted (nitrate-limited) conditions widely observed in the surface layer of the Arctic Ocean (Sakshaug, 2003; Dittmar and Kattner, 2003) also support the inference that biological processes do not control the distribution of surface water pCO_2.

In summary, biological activity was not a primary factor explaining the observed distributions of surface water pCO_2.

4.2 Water mixing

Spatial variations of summertime surface water pCO_2 in the area west of 150° W can be well accounted for by water mixing and cooling of a water mass (Murata and Takizawa, 2003). It is thus possible that the same processes are dominant in the area east of 150° W. To confirm this, we created separate temperature-salinity (T/S) diagrams for 2000 and 2002 (Fig. 7).

BGD
5, 5093–5132, 2008

In general, two types of water mixing can occur. One (type A) is the mixing of waters with high temperature and low salinity, or waters with low temperature and high salinity. The other (type B) is the mixing of high-temperature waters with low-temperature waters, with relatively small variation of salinity. Type A mixing is typical where river discharge to high-latitude seas occurs (Murata, 2006, Else et al., 2008), whereas type B mixing results from the cooling of a water mass (Murata and Takizawa, 2003). The low-temperature water in type B mixing is likely to be derived from melting ice, as it is generally close to the freezing point for a given temperature and salinity.

In the Beaufort Sea, the patterns of water mixing differed between 2000 and 2002. In both 2000 and 2002, type B mixing was seen at relatively high latitudes: on leg 3 in 2000 and legs 1 and 2 in 2002 (Fig. 7). Type A mixing, in contrast, was observed at relatively low latitudes, in particular in the area near the mouth of the Mackenzie River (2002 legs 3 and 5), where type A mixing was clearly dominant (Fig. 7b).

To examine the effects of water mixing on surface water pCO_2, we estimated pCO_2 values calculated from two apparent end members by assuming conservative mixing. Values of the two end members for temperature and salinity were visually selected from the T/S diagrams (Fig. 7) and are listed in Table 4. From each pair of T and S end-member values, together with corresponding values of TCO_2 and TAlk, we computed surface water pCO_2 in relation to salinity at four intermediate points, assuming conservative mixing (Fig. 8). The calculated pCO_2 values well reproduced the observed pCO_2 distributions. In 2002, however, a number of measured surface water pCO_2 values deviated from those computed from the water mixing. These values correspond to the scattered data points at salinity and temperature ranges from 18 to 26 and 0 to 2°C, respectively in the T/S distributions (Fig. 7b). More shipboard observations covering a more extensive area of the coastal region were made in 2002 than in 2000 (Fig. 1), which probably resulted in encounters with more different water mixings.

The dynamic ranges of T and S seen in the T/S diagrams on some legs (Fig. 7) might lead us to expect large changes in pCO_2 when, in fact, the changes in pCO_2 were small. For instance, type B water mixing in 2000 resulted in little variation of

surface water pCO_2 (mixing b; Fig. 8) despite large changes of temperature and salinity (Table 4). This occurs because pCO_2 depends not only on temperature and salinity but also on TCO_2 and TAlk (Takahashi et al., 1993), and river discharge is usually rich in both TCO_2 and TAlk. If it is assumed that the relationships of temperature, salinity, TCO_2, and TAlk with pCO_2 (Takahashi et al., 1993) hold true in the coastal region, the increments of pCO_2, from a beginning value of 270 µatm, due to the changes of temperature, salinity, TCO_2, and TAlk between the end members of mixing b (Table 4) are calculated to be 19, 18, −80, and 35 µatm, respectively, for a net increment of −8 µatm, implying only a small net change in pCO_2. This result demonstrates that small changes in pCO_2 can occur as a result of water mixing.

In conclusion, river discharge is the most important factor accounting for the distributions of surface water pCO_2 in the area east of 150° W. This feature of the pCO_2 distribution is in distinct contrast to that in the area west of 150° W, where no influence of river discharge was detected (Murata and Takizawa, 2003).

4.3 Air-to-sea flux of CO_2

On the basis of the observations during the two years, we investigated spatial variations in the air-sea flux of CO_2 in coastal regions east of 150° W in the Canadian Beaufort Sea, where the influence of river discharge was dominant. In this section, we first discuss differences in the CO_2 fluxes between 2000 and 2002 (Sect. 4.3.1). Second, we investigate differences in the CO_2 fluxes between the areas east and west of 150° W (Sect. 4.3.2). Then, we attempt to estimate air-to-sea CO_2 fluxes in an extended area in the ice-free season, and we compare the results with those obtained by previous studies (Sect. 4.3.3).

4.3.1 Differences between 2000 and 2002

Although the mean CO_2 flux did not show large differences between 2000 and 2002, distinct differences in the variability of the CO_2 flux were observed between the two

years. Variability was larger in 2002 (Sect. 3.2), probably because the wind speed frequency distributions differed (Fig. 9). The wind speed frequency distribution in 2000 was unimodal, with one peak at the wind speed class of 6–7 $m\,s^{-1}$, whereas the distribution in 2002 was bimodal, with peaks at wind speed classes of 4–5 and 12–13 $m\,s^{-1}$. This difference in the wind speed frequency distributions is reflected in the frequency distributions of the CO_2 fluxes (Fig. 10). In 2000 (Fig. 10a), the CO_2 fluxes were concentrated in a few frequency classes, whereas in 2002, they showed a wider range (Fig. 10b). In spite of this difference, 86% and 76% of the total CO_2 flux ranged from -30 to 0 $mmol\,m^{-2}\,d^{-1}$ in 2000 and 2002, respectively, resulting in the nearly equal means of the CO_2 flux.

4.3.2 Differences between the areas east and west of 150° W

To compare the CO_2 fluxes in the area east of 150° W with those observed west of 150° W, we calculated the CO_2 fluxes from data obtained west of 150° W during cruises MR00-K06 and MR02-K05. The CO_2 fluxes during MR00-K06 were previously calculated by Murata and Takizawa (2003). However, we recalculated them, because Murata and Takizawa (2003) used averaged wind speeds to calculate the CO_2 fluxes, which moderated their spatial and temporal variability.

The averaged CO_2 fluxes in the area west of 150° W (Table 5) were almost equivalent to those in the area east of 150° W (Table 3). Furthermore, the shapes of the CO_2 flux frequency distributions were similar between east and west of 150° W (compare Fig. 10a and b with Fig. 10c and d, respectively); the CO_2 fluxes mostly range from -30 to 0 $mmol\,m^{-2}\,d^{-1}$ in both areas. The frequencies of CO_2 fluxes outside this range were quite small. These findings indicate that the absorption of CO_2 by the ocean was almost equivalent between the areas.

Although the high-frequency parts of the distributions displayed an overall accordance, extreme CO_2 flux values were positive east of 150° W, whereas west of 150° W, they were negative. Positive extreme values were observed chiefly in 2002, and co-

BGD
5, 5093–5132, 2008

incided with the elevated surface water pCO_2 values (Fig. 3a), which were probably caused by upwelling of subsurface waters rich in CO_2. Vertical distributions of water temperature and salinity at the time of the large positive CO_2 fluxes indicate that upwelling of lower temperature and saltier water brought up water rich in CO_2 (Fig. 11). Upwelling conditions, however, returned shortly (after about 2 h) to the usual conditions (higher temperature and lower salinity water; Fig. 11). Williams et al. (2008) reported that conditions favorable to upwelling often occur in the area, depending on wind direction, supporting our inference. In fact, changes in wind direction were recorded during the cruise. On the other hand, the large negative CO_2 fluxes west of 150° W were probably associated with decreases in surface water pCO_2 caused by water mixing and cooling (Murata and Takizawa, 2003; Bates, 2006), together with high wind speeds.

4.3.3 Air-to-sea CO_2 fluxes and comparison with previous studies

As discussed in Sect. 4.2, surface water pCO_2 in the area east of 150° W showed spatial variability associated with river discharge, but that in the area west of 150° W did not (Murata and Takizawa, 2003). In spite of the different mechanisms causing spatial variability, the means and frequency distributions of the CO_2 fluxes were similar between the two areas (Sect. 4.3.2). Therefore, we adopted values of −30 to 0 mmol m^{-2} d^{-1} as representative CO_2 flux values for the region as a whole (165°–130° W; 70°–73° N). Our observations were made chiefly in September, when the ice-free area is at its maximum. Bates (2006) estimated CO_2 fluxes during spring (May–June) to summer (July–August) to be –30 to –90 mmol m^{-2} d^{-1}, using observations made in 2002. On the basis of observations made in August–September 1996, Pipko et al. (2002) reported that surface water pCO_2 in the Chukchi Sea was mainly undersaturated in CO_2 with respect to the atmosphere and that the averaged CO_2 flux was −12.2 mmol m^{-2} d^{-1}. These results indicate that the region as a whole acts as a sink for atmospheric CO_2 throughout the year, if the air-sea flux of CO_2 during the ice-covered season is neglected.

BGD
5, 5093–5132, 2008

They also imply that on a seasonal time scale, no mechanisms causing CO_2 source conditions exist in the region, although source conditions occur over a shorter (meso) time scale near the mouth of the Mackenzie River (Sect. 4.3.2). However, because of the low frequency of sea-to-air CO_2 fluxes (Fig. 10), for estimations on a seasonal or annual basis, these CO_2 fluxes can be ignored. From the estimated CO_2 flux of $-10.2\pm7.7\,mmol\,m^{-2}\,d^{-1}$, calculated from all flux values from -30 to $0\,mmol\,m^{-2}\,d^{-1}$, the area of the combined region (= $411\,000\,km^2$), and the assumed ice-free period (= 100 days), we estimated the uptake of CO_2 in the entire region during the ice-free period to be $5.0\pm3.8\,Tg\,C$.

The CO_2 flux estimated in the present study ($-10.2\,mmol\,m^{-2}\,d^{-1}$) is close to that ($-12.2\,mmol\,m^{-2}\,d^{-1}$) reported by Pipko et al. (2002), but smaller than those (-30 to $-90\,mmol\,m^{-2}\,d^{-1}$) reported by Bates (2006), both of whom based their calculations on the formulation of W92. The different results probably reflect seasonal differences. The observations of the present study and those of Pipko et al. (2002) were obtained in late summer, while those of Bates (2006) were obtained from spring to early summer. In spring to early summer, enhanced biological activity such as blooms operate to reduce surface water pCO_2 considerably, causing larger air-to-sea CO_2 fluxes.

The CO_2 flux estimated in the present study is also close to values found in other high-latitude marginal seas: $-1.94\,mol\,C\,m^{-2}\,yr^{-1}$ (Borges et al., 2005) and $-12\,g\,C\,m^{-2}\,yr^{-1}$ (Cai et al., 2006).

4.4 Capacity of the Beaufort Sea as a CO_2 sink

The buffer factor, that is, the ratio of the change in pCO_2 to that in TCO_2, generally ranges from 9 to 13 in open oceans (Takahashi et al., 1993; Sabine et al., 2004) and is often used to evaluate oceanic capacity as a CO_2 sink: the lower the buffer factor, the larger the potential for CO_2 uptake. In fact, more anthropogenic CO_2 is stored in the subtropical oceans, where the buffer factor is lower, than in the polar oceans, where the buffer factor is higher (Sabine et al., 2004). In this section, we use the buffer factor

to evaluate the capacity of the study area as a CO_2 sink during the ice-free season.

To estimate the buffer factor, we first computed pCO_2 at an average temperature and a salinity of 35 from $nTCO_2$ and TAlk normalized to a salinity of 35 (nTAlk), using the same combination of constants as used for the TAlk calculation (Sect. 2.2). Then, we calculated the natural logarithms of $nTCO_2$ ($\ln(nTCO_2)$) and of the calculated pCO_2 ($\ln(pCO_2)$). Distributions of the $\ln(pCO_2)$ as a function of the $\ln(nTCO_2)$ are illustrated in Fig. 12a and b. The buffer factor corresponds to the slope of the regression line.

In both years, the calculated buffer factor east of 150° W was 1.5. The buffer factor west of 150° W, however, calculated by the same method (Fig. 12c and d), was 6.9 in 2000 and 5.2 in 2002, although the fit of the regression lines is relatively poor. Furthermore, two separate trends can be discerned visually in 2002, suggesting the presence of different water masses in the area. Bates (2006) reported low buffer factors of ~3.5–6.5 in the area of 170°–150° W, 65°–75° N in summer 2002, which are close to the values that we obtained in the area west of 150° W. The buffer factors obtained in the area east of 150° W are much lower, implying that there is a higher potential sink for atmospheric CO_2 in that area.

The difference in the buffer factors between the areas probably originates from differences in water masses. As discussed so far, the area east of 150° W is influenced by river discharge, but not the area west of 150° W (Murata and Takizawa, 2003). Thus the extremely low buffer factors obtained east of 150° W probably reflect the carbonate system of water masses affected by river discharge. The extremely low values were probably caused by a decrease in $nTCO_2$ with little change in nTAlk, which are features of biological production (decreases of $nTCO_2$) along with an absence of calcification (no changes of $nTCO_2$). Bates (2006) similarly explained the low buffer factor in the area west of 150° W. As examined in Sect. 4.1, biological activity was not efficient in the area east of 150° W, although biological activity occurring in upstream of rivers may cause the buffer factor to be low in the area.

5 Concluding remarks

We discussed spatial variations of surface water pCO_2 and the air-sea flux of CO_2 in coastal regions of the Canadian Beaufort Sea. The spatial variations in pCO_2 were primarily associated with water mixing, related chiefly to river discharge. Biological processes seemed to be of minor importance during this late summer season. Overall, the area acted a moderate sink for atmospheric CO_2.

The influence of river discharge was well confirmed by vertical distributions of $nTCO_2$, nTAlk, and other physical and chemical properties. Namely, distinct vertical gradients in these properties were found in the top few tens of meters. These vertical gradients, however, also raise some questions, because similar vertical gradients in these properties often occur also in the top few meters, implying that their values at the sea surface may differ from those a few meters below. For air-sea exchange, values at the sea surface are important. During the cruises, we collected surface water samples at nearly 0 m by using a bucket. At one CTD station (69° 45.04′ N; 138° 09.44′ W), for instance, surface salinity, water temperature, TCO_2, and TAlk by bucket sampling were 17.80, 2.1°C, 1860.9 µmol kg^{-1}, and 1941.1 µmol kg^{-1}, respectively. Using these values, we calculated surface water pCO_2 to be 284.6 µatm. The observed surface water pCO_2, in water sampled from about 4 m depth, was 333.1±3.3 µatm. This difference of about 48 µatm is not negligible. We cannot explain why a large vertical difference in pCO_2 existed between the sea surface and the depth of approximately 4 m. Nevertheless, since the water temperature and salinity values obtained by the bucket sampling were not markedly different from the averaged values of the continuous measurements, which were 2.00°C and 17.21, respectively, biological processes in the thin surface layer may possibly account for the difference in pCO_2 within the top 4 m.

The vertical difference in pCO_2, which has been left unexamined so far, probably affects the calculated air-sea flux of CO_2. Further studies are necessary to investigate this point.

BGD
5, 5093–5132, 2008

Acknowledgements. We thank the officers and crew of the R/V *Mirai* for exceptional support during the cruises. We also give special thanks to the staff of Marine Works Japan, who worked as physical and chemical oceanography marine technicians on board the R/V *Mirai,* and who also worked to ensure that the data obtained by the shipboard observations were of the first quality.

References

Bates, N. R.: Air-sea CO_2 fluxes and the continental shelf pump of carbon in the Chukchi Sea adjacent to the Arctic Ocean, J. Geophys. Res., 111, C10013, doi:10.1029/2005JC003083, 2006.

Bates, N. R., Best, M. H. P., and Hansell, D. A.: Spatio-temporal distribution of dissolved inorganic carbon and net community production in the Chukchi and Beaufort Seas, Deep-Sea Res. II, 52, 3303–3323, 2005.

Bates, N. R., Moran, S. B., Hansell, D. A., and Mathis, J. T.: An increasing CO_2 sink in the Arctic Ocean due to sea-ice loss, Geophys. Res. Lett., 33, L23609, doi:10.1029/2006GL027028, 2006.

Borges, A. V. Delille, B., and Frankignoulle, M.: Budgeting sinks and sources of CO_2 in the coastal ocean: Diversity of ecosystems counts, Geophys. Res. Lett., 32, L14601, doi:10.1029/2005GL023053, 2005.

Cai, W.-J., Dai, M., and Wang, Y.: air-sea exchange of carbon dioxide in ocean margins: A province-based synthesis, Geophys. Res. Lett., 33, L12603, doi:10.1029/2006GL026219, 2006.

Coachman, L. K., Aagaard, K., and Tripp, R. B.: Bering Strait: The Regional Physical Oceanography, Univ. of Washington Press, Seattle and London, 172 pp., 1975.

Codispoti, L. A., Friederich, G. E., and Hood, D. W.: Variability in the inorganic carbon system over the southeastern Bering Sea shelf during spring 1980 and spring-summer 1981, Cont. Shelf Res., 5, 133–160, 1986.

Dickson, A. G.: Thermodynamics of the dissociation of boric acid in synthetic seawater from 273.15 to 318.15 K, Deep-Sea Res., 37, 755–756, 1990a.

Dickson, A. G.: Standard potential of the reaction: $AgCl(s)+1/2H_2(g)=Ag(s)+HCl(aq)$, and the

standard acidity constant of the ion HSO_4^- in synthetic sea water from 273.15 to 318.15 K, J. Chem. Thermodyn., 22, 113–127, 1990b.
Dickson, A. G. and Riley, J. P.: The estimation of acid dissociation constants in seawater media from potentiometric titrations with strong base. I. The ionic product of Water (K_W), Mar. Chem., 7, 89–99, 1979.
Dittmar, T. and Kattner, G.: The biogeochemistry of the river and shelf ecosystem of the Arctic Ocean: a review, Mar. Chem., 83, 103–120, 2003.
Else, B. G. T., Papakyriakou, T. N., Granskog, M. A., and Yackel, J. J.: Observations of sea surface fCO_2 distributions and estimated air-sea CO_2 fluxes in the Hudson Bay region (Canada) during the open-water season, J. Geophys. Res., 113, C08026, doi:10.1029/2007JC004389, 2008.
Emmerton, C. A., Lesack, L. F. W., and Vincent, W. F.: Mackenzie River nutrient delivery to the Arctic Ocean and effects of the Mackenzie Delta during open water conditions, Global Biogeochem. Cy., 22, GB1024, doi:10.1029/2006GB002856, 2008.
Goyet, C. and Poisson, A.: New determination of carbonic acid dissociation constants in seawater as a function of temperature and salinity, Deep-Sea Res., 36, 1635–1654, 1989.
Hansell, D. A. and Carlson, C. A.: Net community production of dissolved organic carbon, Global Biogeochem. Cy., 12, 443–453, 1998.
Ho, D. T., Law, C. S., Smith, M. J., Scholsser, P., and Harvey, M.: Measurements of air-sea gas exchange at high wind speeds in the Southern Ocean: Implications for global parameterizations, Geophys. Res. Lett., 33, L16611, doi:10.1029/2006GL026817, 2006.
Ishii, M., Inoue, H. Y., Matsueda, H., and Tanoue, E.: Close coupling between seasonal biological production and dynamics of dissolved inorganic carbon in the Indian Ocean sector and the western Pacific Ocean sector of the Antarctic Ocean, Deep-Sea Res. I, 45, 1187–1209, 1998.
Le Quéré, C., Orr, J. C., Monfray, P., and Aumont, O.: Interannual variability of the oceanic sink of CO_2 from 1979 through 1997, Global Biogeochem. Cy., 14(4), 1247–1265, 2000.
Lewis, E. and Wallace, D. W. R.: Program developed for CO_2 system calculations, Carbon Dioxide Information Analysis Center, Report ORNL/CMDL-105, Oak Ridge National Laboratory, Oak Ridge, TN, 1998.
Liss, P. S. and Merlivat, L.: Air-sea gas exchange rates: introduction and synthesis, in: The Role of air-sea Exchange in Geochemical Cycling, edited by: Buat-Menard, P., NATO ASI Series C: Mathematical and Physical Science, 185, 113–128, 1986.

Midorikawa, T., Umeda, T., Hiraishi, N., Ogawa, K., Nemoto, K., Kudo, N., and Ishii, M.: Estimation of seasonal net community production and air-sea CO_2 flux based on the carbon budget above the temperature minimum layer in the western subarctic North Pacific, Deep-Sea Res. I, 49, 339–362, 2002.

Millero, F. J.: Thermodynamics of the carbon dioxide system in the ocean, Geochim. Cosmochim. Acta, 59, 661–677, 1995.

Murata, A.: Increased surface seawater pCO_2 in the eastern Bering Sea shelf: An effect of blooms of coccolithophorid *Emiliania huxleyi*?, Global Biogeochem. Cy., 20, GB4006, doi:10.1029/2005GB002615, 2006.

Murata, A. and Takizawa, T.: Summertime CO_2 sinks in shelf and slope waters of the western Arctic Ocean, Cont. Shelf Res., 23, 753–776, 2003.

Murata, A., Kumamoto, Y., Saito, C., Kawakami, H., Asanuma, I., Kusakabe, M., and Inoue, H. Y.: Impact of a spring phytoplankton bloom on the CO_2 system in the mixed layer of the northwestern North Pacific, Deep-Sea Res. II, 49, 5531–5555, 2002.

Nightingale, P. D., Malin, G., Law, C. S., Watson, A. J., Liss, P. S., Liddicoat, M. I., Boutin, J., and Upstill-Goddard, R. C.: In situ evaluation air-sea gas exchange parameterization using novel conservative and volatile tracers, Global Biogeochem. Cy., 14, 373–387, 2000.

Obata, A. and Kitamura, Y.: Interannual variability of sea-air exchange of CO_2 from 1961 to 1998 with a global ocean circulation biogeochemistry model, J. Geophys. Res., 108(C11), 3337, doi:10.1029/2001JC001088, 2003.

Pipko, I. I., Semiletov, I. P., Tishchenko, P., Ya, Pugach, S. P., and Christensen, J. P.: Carbonate chemistry dynamics in Bering Strait and the Chukchi Sea, Prog. Oceanogr., 55, 77–94, 2002.

Rothrock, D. A., Yu, Y., and Maykut, G. A.: Thinning of the Arctic sea ice cover, Geophys. Res. Lett., 26(23), 3469, doi:10.1029/1999GL010863, 1999.

Sabine, C. L., Feely, R. A., Gruber, N., Key, R. M., Lee, K., Bullister, J. L., Wanninkhof, R., Wong, C. S., Wallace, D. W., Tilbrook, B., Millero, F. J., Peng, T.-H., Kozyr, A., Ono, T., and Rios, A. F.: The oceanic sink for anthropogenic CO_2, Science, 305, 367–371, 2004.

Sakshaug, E.: Primary and secondary production in the Arctic Sea, in: The Organic Carbon Cycle in the Arctic Ocean, edited by: Stein, R. and Macdonald, R. W., Springer-Verlag, Berlin, 57–81, 2003.

Schlitzer, R.: Ocean Data View, available at: http://www.awi-bremerhaven.de/GEO/ODV/(last access: 19 September, 2007), 2001.

Solomon, S., Qin, D., Manning, M., Alley, R. B., Berntsen, T., Bindoff, N. L., Chen, Z., Chidtaisong, A., Gregory, J. M., Hegerl, G. C., Heimann, M., Hewitson, B., Hoskins, B. J., Joos, F., Jouzel, J., Kattsov, V., Lohmann, U., Matsuno, T., Molina, M., Nicholls, N., Overpeck, J., Raga, G., Ramaswamy V., Ren, J., Rusticucci, M., Somerville, R., Stocker, T. F., Whetton, P., Wood, R. A., and Wratt, D.: Technical summary, in: Solomon, S., Qin, D., Manning, M., Chen, Z., Marquis, M., Averyt, K. B., Tignor, M., and Miller, H. L. (Eds.): Climate Change 2007: The Physical Science Basis, Contribution of Working Group I to the Fourth Assessment Report of the Intergovernmental Panel on Climate Change, Cambridge University Press, Cambridge, United Kingdom and New York, USA, 2007.

Stroeve, J. C., Serreze, M. C., Fetterer, F., Arbetter, T., Meier, W., Maslanik, J., and Knowles, K.: Tracking the Arctic's shrinking ice cover: Another extreme September minimum in 2004, Geophys. Res. Lett., 32, L04501, doi:10.1029/2004GL021810, 2005.

Takahashi, T., Olafsson, J., Goddard, J. G., Chipman, D. W., and Sutherland, S. C.: Seasonal variations of CO_2 and nutrients in the high-latitude surface oceans: A comparative study, Global Biogeochem. Cy., 7, 843–878, 1993.

Takahashi, T., Sutherland, S. C., Sweeney, C., Poisson, A., Metzl, N., Tilbrook, B., Bates, N., Wanninkhof, R., Feely, R. A., Sabine, C., Olafsson, J., and Nojiri, Y.: Global sea-air CO_2 flux based on climatological surface ocean pCO_2, and seasonal biological and temperature effects, Deep Sea Res. II, 49, 1601–1622, 2002.

Tans, P. P. and Conway, T. J.: Monthly atmospheric CO_2 mixing ratios from the NOAA CMDL Carbon Cycle Cooperative Global Air Sampling Network, 1968–2002, in: Trends: A Compendium of Data on Global Change, Carbon Dioxide Information Analysis Center, Oak Ridge National Laboratory, US Department of Energy, Oak Ridge, Tenn., USA, 2005.

Valiela, I.: Marine Ecological Processes, Springer, Tokyo, 686 pp., 1995.

Wanninkhof, R.: Relationship between wind speed and gas exchange over the ocean, J. Geophys. Res., 97, 7373–7382, 1992.

Wanninkhof, R. and McGills, W. R.: A cubic relationship between air-sea CO_2 exchange and wind speed, Geophys. Res. Lett., 26, 1889–1892, 1999.

Weiss, R. F.: Carbon dioxide in water and seawater: the solubility of a non-ideal gas, Mar. Chem., 2, 203–215, 1974.

Weiss, R. F. and Price, B. A.: Nitrous oxide solubility in water and seawater, Mar. Chem., 8, 347–359, 1980.

Wetzel, P., Winguth, A., and Maier-Reimer, E.: Sea-to-air CO_2 flux from 1948 to 2003: A mode study, Global Biogeochem. Cy., 19, GB2005, doi:10.1029/2004GB002339, 2005.
Williams, W. J., Melling, H., Carmack, E. C., and Ingram, R. G.: Kugmallit Valley as a conduit for cross-shelf exchange on the Mackenzie Shelf in the Beaufort Sea, J. Geophys. Res., 113, C02007, doi:10.1029/2006JC003591, 2008.

Table 1. Comparison between atmospheric CO_2 in the area east of 150° W during cruises MR00-K06 (n=248) and MR02-K05 (n=429), and the monthly mean (± standard deviation) atmospheric CO_2 in September, measured at Point Barrow (71° 32′ N, 156° 60′ W) (Tans and Conway, 2005).

Cruise	Period (UTC)	xCO_2 (ppmv)	pCO_2 (µatm)	CO_2 at Point Barrow (ppmv)
MR00-K06	1–22 Sep 2000	363.2±1.8	361.0±1.8	361.90
MR02-K05	15–30 Sep 2002	367.0±1.4	364.7±1.4	365.29

Table 2. Means (± standard deviation), maxima, and minima of surface water pCO_2 during MR00-K06 (n=855) and MR02-K05 (n=1711).

Cruise	Period	Mean (µatm)	Max. (µatm)	Min. (µatm)
MR00-K06	13–22 Sep 2000	292.1±22.1	395.4	261.2
MR02-K05	15–30 Sep 2002	306.5±27.6	490.0	252.6

Table 3. Means of ΔpCO_2 and the CO_2 fluxes in the area east of 150° W.

Cruise	ΔpCO_2(µatm)	CO_2 flux (mmol m^{-2} d^{-1})				
		W92[1]	LM86[2]	WM99[3]	N00[4]	H06[5]
MR00-K06	−68.3±22.2	−15.0±11.3	−8.6±5.9	−13.8±14.1	−11.9±8.5	−12.3±9.2
MR02-K05	−58.2±27.6	−16.8±20.0	−9.1±10.6	−18.9±28.9	−13.0±14.9	−13.7±16.3

[1] Wanninkhof (1992)
[2] Liss and Merlivat (1986)
[3] Wanninkhof and McGillis (1999)
[4] Nightingale et al. (2000)
[5] Ho et al. (2006)

Table 4. End-member values of water temperature (T), salinity (S), TCO_2, and TAlk for various types of conservative water mixing.

Cruise	Mixing	T (°C)	S	TCO_2 (μmol kg^{-1})	TAlk (μmol kg^{-1})
MR00-K06	a	2.432 (−0.979)	15.43 (24.84)	1867.9 (1798.1)	1924.5 (1875.9)
	b	−0.420 (1.268)	26.61 (28.42)	1817.0 (1899.3)	1914.6 (2024.9)
MR02-K05	c	3.765 (−0.382)	11.48 (28.46)	1677.2 (1691.4)	1724.3 (1748.6)
	d	2.488 (−0.382)	16.40 (28.46)	1691.4 (1930.6)	1748.6 (2048.4)
	e	2.907 (−0.972)	23.97 (25.99)	1684.1 (1802.5)	1767.1 (1879.7)
	f	1.331 (−1.000)	26.04 (26.04)	1784.7 (1784.7)	1863.2 (1863.2)
	g	1.297 (1.220)	14.56 (23.35)	1715.1 (1686.6)	1754.3 (1758.0)

Values in parentheses indicate the second end-member are first end member values; values without parentheses are the first end-member values.

BGD
5, 5093–5132, 2008

Table 5. Means of ΔpCO_2 and the CO_2 fluxes in the area west of 150° W.

Cruise	ΔpCO_2 (µatm)	CO_2 flux (mmol m^{-2} d^{-1})				
		W92[1]	LM86[2]	WM99[3]	N00[4]	H06[5]
MR00-K06	−102.6±34.0	−16.8±14.4	−9.7±8.0	−14.8±17.8	−13.5±10.9	−13.8±11.8
MR02-K05	−70.0±27.4	−17.3±23.4	−9.5±12.5	−20.7±40.1	−13.4±17.2	−14.2±19.1

[1] Wanninkhof (1992)
[2] Liss and Merlivat (1986)
[3] Wanninkhof and McGillis (1999)
[4] Nightingale et al. (2000)
[5] Ho et al. (2006)

BGD
5, 5093–5132, 2008

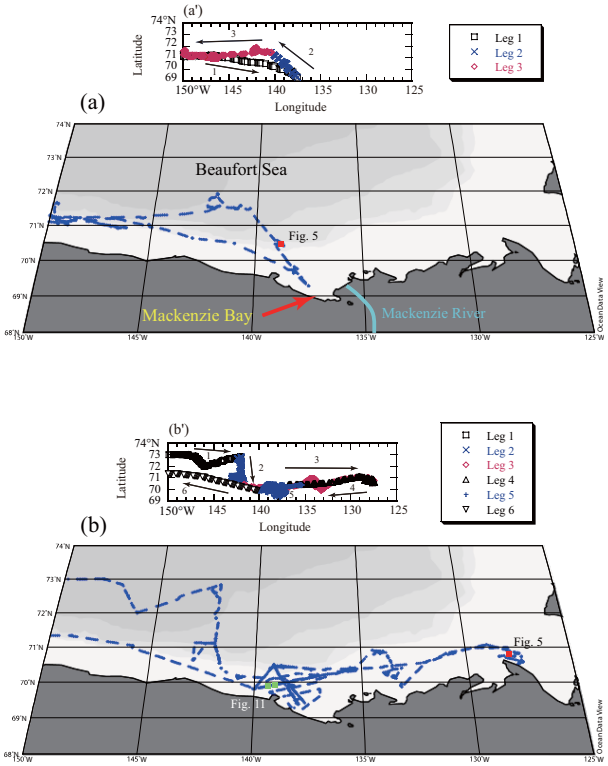

Fig. 1. Cruise areas during **(a)** MR00-K06 (2000) and **(b)** MR02-K05 (2002). Solid circles show points where surface water pCO_2 was sampled. The locations of CTD water sampling stations in 2000 and 2002, from which the data in Figs. 5 and 11 were obtained, are indicated by red and light-green squares, respectively. This map was created with ODV Software (Schlitzer, 2001). The numbers in panels **(a')** and **(b')** indicate leg numbers and are associated with the numbers of Figs. 2, 3, 4, and 7. Arrows in the panels indicate the sailing direction.

BGD
5, 5093–5132, 2008

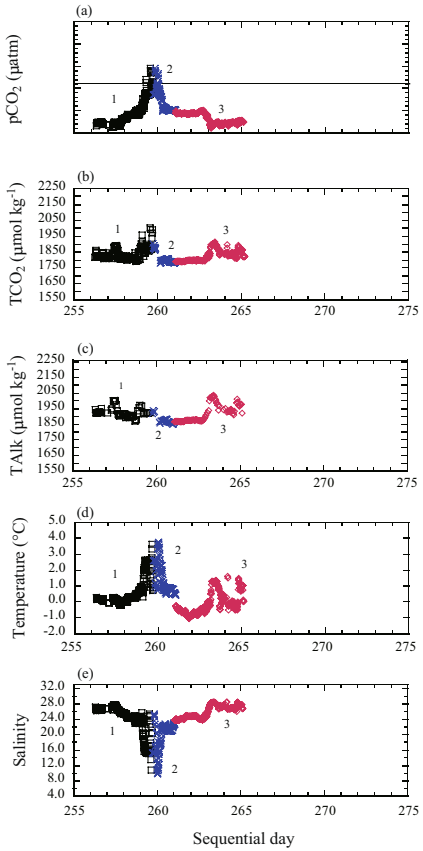

Fig. 2. **(a)** Distributions of **(a)** surface water pCO_2, and **(b)** surface water TCO_2, **(c)** surface water TAlk, **(d)** SST, and **(e)** SSS as a function of sequential day during cruise MR00-K06. The distributions of each property are shown in different colors, according to portions (legs 1–3) of the cruise, which correspond to the observation points in Fig. 1a'. In panel (a), the horizontal line indicates the mean atmospheric pCO_2 (361.0 µatm).

BGD
5, 5093–5132, 2008

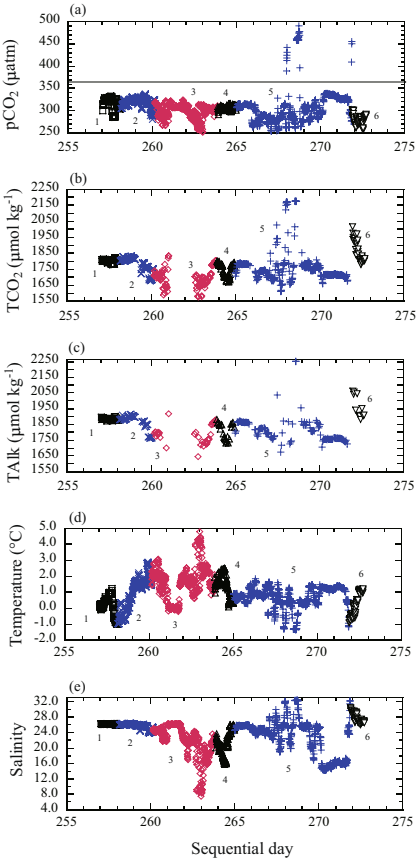

Fig. 3. Distributions of **(a)** surface water pCO_2, **(b)** surface water TCO_2, **(c)** surface water TAlk, **(d)** SST, and (e) SSS as a function of sequential day during cruise MR02-K05. The distributions of each property are shown in different colors, according to legs 1–6 of the cruise, which correspond to the observation points in Fig. 1b'. In panel (a), the horizontal line indicates the mean atmospheric pCO_2 (364.7 µatm).

BGD
5, 5093–5132, 2008

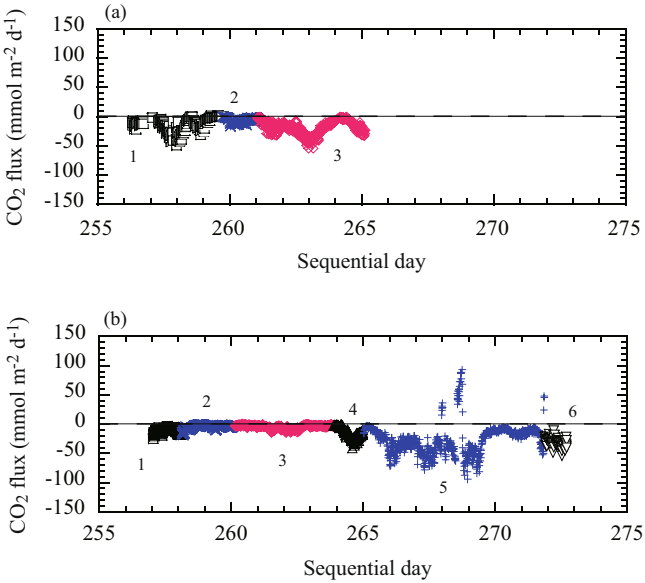

Fig. 4. Distributions of the CO_2 fluxes calculated based on the W92 formulation as a function of sequential day for **(a)** MR00-K06 and **(b)** MR02-K05. The distributions of the CO_2 fluxes during legs 1–3 of MR00-K06 and legs 1–6 of MR02-K05 correspond to the observation points shown in panels **(a')** and **(b')** in Fig. 1, respectively.

BGD
5, 5093–5132, 2008

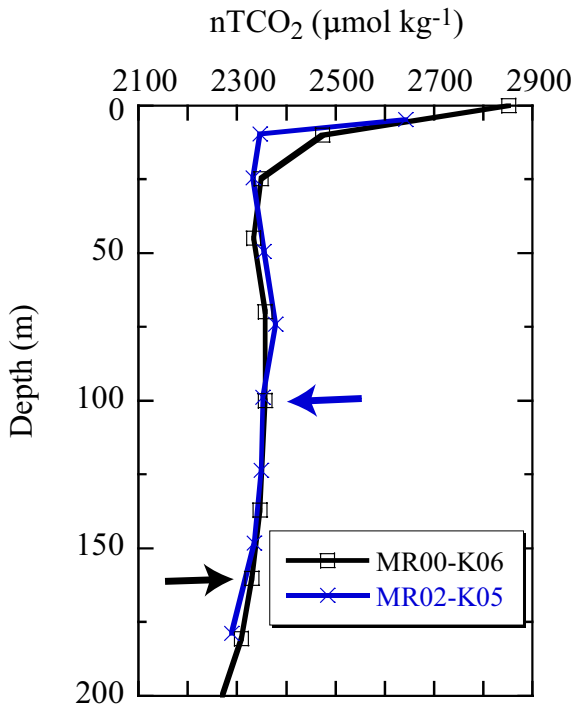

Fig. 5. Vertical distribution of $nTCO_2$ during MR00-K06 (squares) and MR02-K05 (crosses). Arrows indicate the temperature minimum layer in each vertical profile. The observation points are shown in Fig. 1.

BGD
5, 5093–5132, 2008

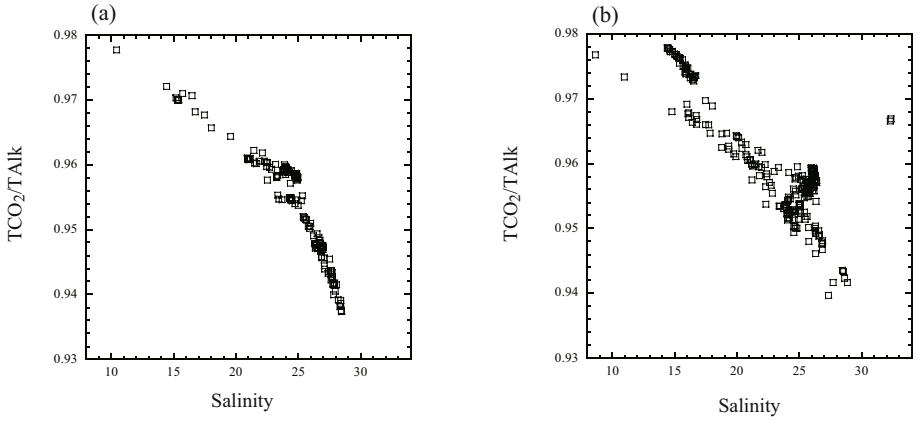

Fig. 6. Distributions of TCO_2/TAlk as a function of salinity for **(a)** MR00-K06 and **(b)** MR02-K05.

BGD
5, 5093–5132, 2008

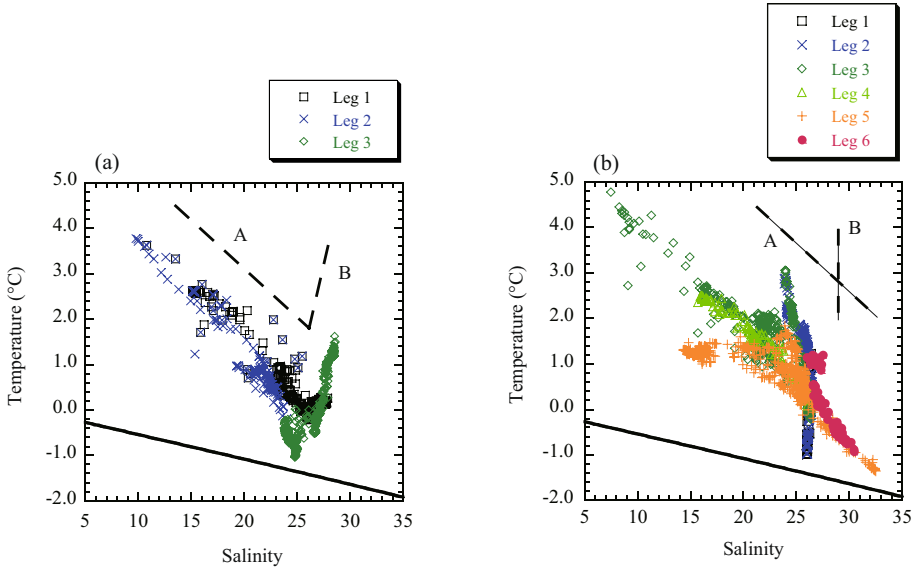

Fig. 7. T/S diagrams for **(a)** MR00-K06 and **(b)** MR02-K05. The distributions are divided according to the cruise legs, shown by different colors, as in Fig. 1a' and b'. The solid line in each panel indicates the freezing point at a given temperature and salinity. The broken lines show the two mixing types (A and B) schematically.

BGD
5, 5093–5132, 2008

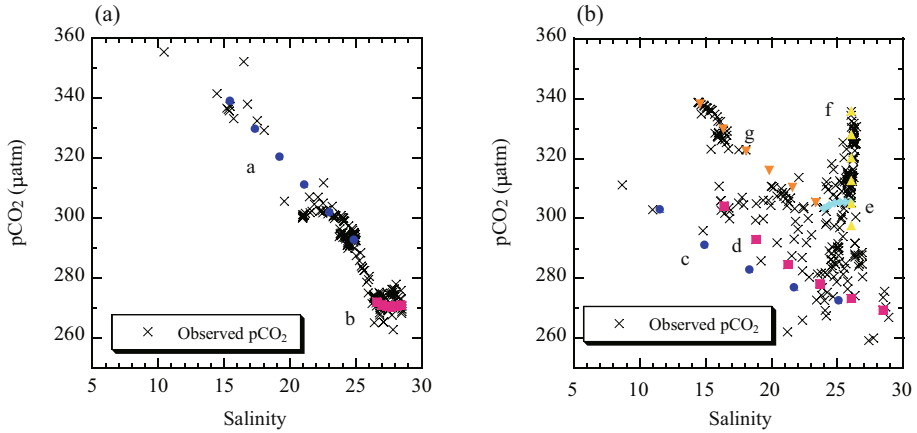

Fig. 8. Distributions of observed (crosses) and calculated (colored symbols labeled with letters a–g) pCO_2 as a function of salinity for **(a)** MR00-K06 and **(b)** MR02-K05. Calculated pCO_2 values are based on the conservative mixing of two end members, which are given in Table 4.

BGD
5, 5093–5132, 2008

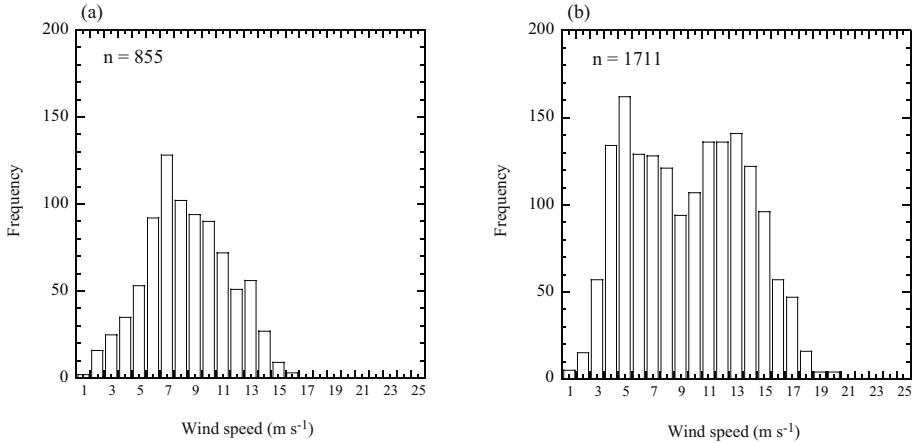

Fig. 9. Frequency distributions of wind speed for **(a)** MR00-K06 and **(b)** MR02-K05.

BGD
5, 5093–5132, 2008

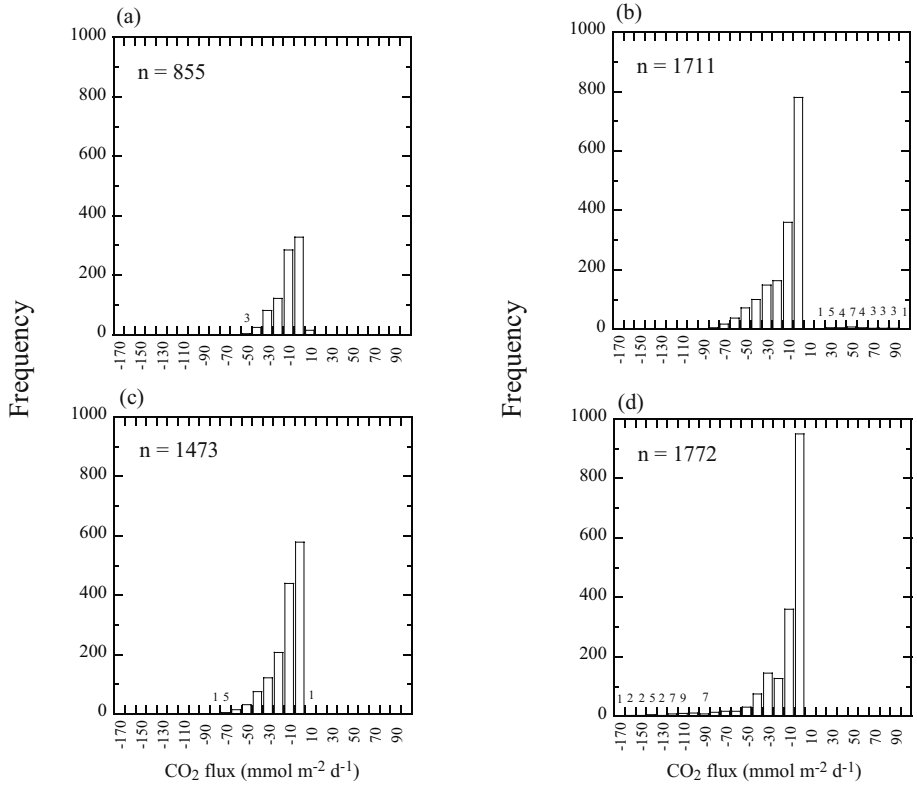

Fig. 10. Frequency distributions of the CO_2 fluxes calculated based on the W92 formulation in the area east of 150° W for **(a)** MR00-K06 and **(b)** MR02-K05, and the area west of 150° W for **(c)** MR00-K06 and **(d)** MR02-K05. For frequencies less than 10, the columns are labeled with the number of observations for clarity.

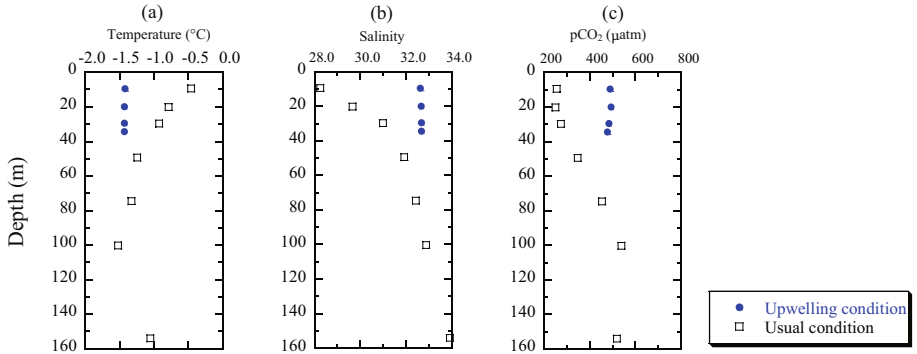

Fig. 11. Vertical distributions of **(a)** temperature, **(b)** salinity, and **(c)** calculated pCO_2 under upwelling (solid circles) and usual (squares) conditions. The observation points are shown in Fig. 1.

BGD
5, 5093–5132, 2008

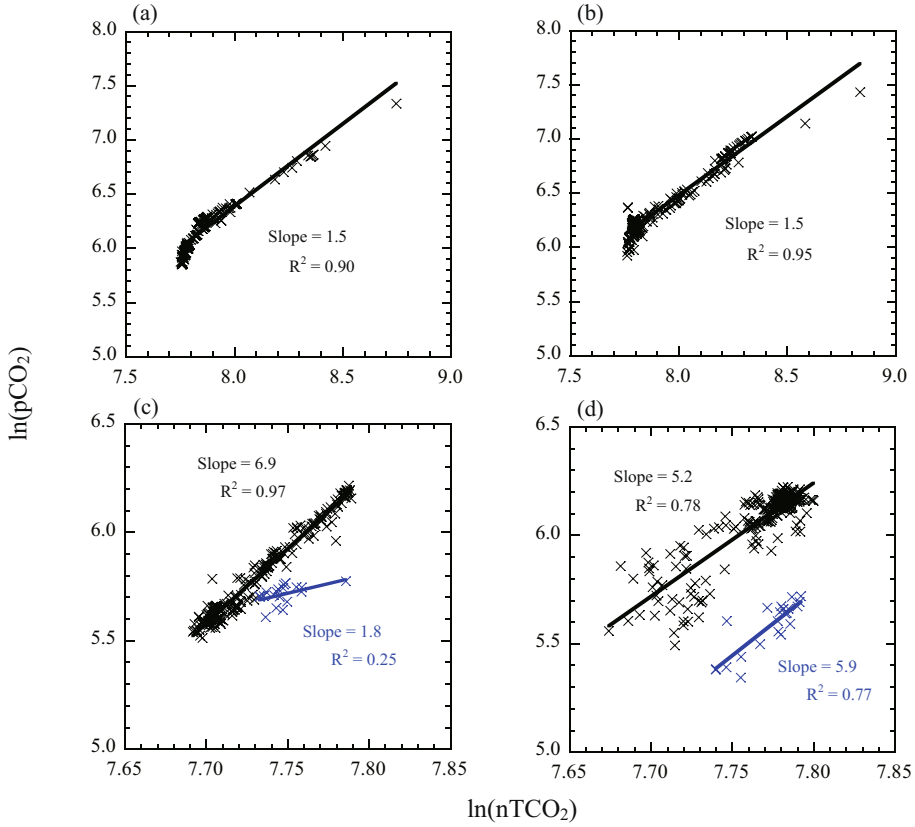

Fig. 12. Buffer factors calculated from the slopes of regression lines of $\ln(pCO_2)$ regressed on $\ln(nTCO_2)$ for the area east of 150° W during **(a)** MR00-K06 and **(b)** MR02-K05, and for the area west of 150° W during **(c)** MR00-K06 and **(d)** MR02-K05.

BGD
5, 5093–5132, 2008